Structural Correlations in Jahn-Teller Systems of Mn^{3+} and Cu^{2+}: Unraveling Local Structures through Spectroscopic Techniques

Marina T. Candela[a], Enrique Jara[b], Fernando Aguado[b], Rafael Valiente[a], Fernando Rodríguez[b,]*

[a]Applied Physics Department, Facultad de Ciencias, University of Cantabria, 39005 Santander, Spain

[b]MALTA Consolider Team, Earth Science and Condensed Matter Physics Department (DCITIMAC), Facultad de Ciencias, University of Cantabria, 39005 Santander, Spain.

* Corresponding author: Fernando Rodríguez

E-mail: rodriguf@unican.es

Supporting Information Content

1. Electronic *d*-orbital structure of Cu^{2+} in $KZnF_3:Cu^{2+}$ and $K_2ZnF_4:Cu^{2+}$ from optical spectroscopy.

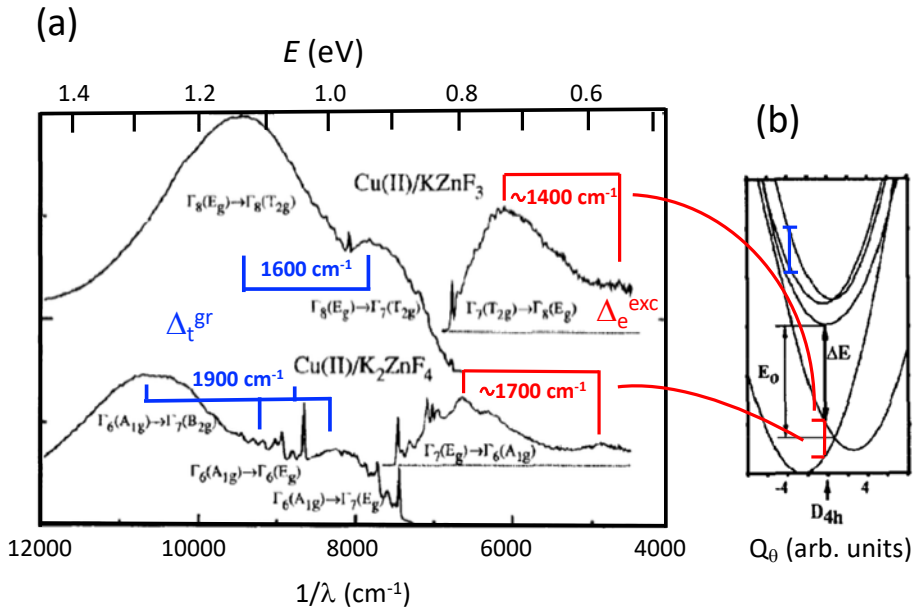

Figure S1

(a) Low-temperature emission and excitation spectra of $KZnF_3:Cu^{2+}$ and $K_2ZnF_4:Cu^{2+}$ showing a double-band structure associated mainly with the splitting of the parent octahedral e_g (red) and t_{2g} (blue) orbitals, Δ_e and Δ_t caused by the low-symmetry JT distortion of the CuF_6 polyhedron. Note that the splitting in excitation corresponds to the splitting of the octahedral $^2T_{2g}$ excited state at the equilibrium geometry of the ^2E_g ground state distorted by the Jahn-Teller effect ($E\otimes e$) and crystal anisotropy (in K_2ZnF_4): Δ_t^{gs}. In the emission spectra, the observed double band structure corresponds to transitions from the $^2T_{2g}$ excited state to the octahedral ^2E_g ground state split by the low-symmetry crystal field at the equilibrium geometry of the excited state ($E\otimes t$): Δ_e^{es}. It must be noted that observed emission splitting in emission, named Δ_e^{es}, corresponds to the tetragonal splitting of the octahedral e_g orbitals at the excited-state equilibrium geometry. It is different from the splitting $\Delta_e = \Delta_e^{gs}$ observed in absorption as it does really correspond to the e_g splitting at the ground-state equilibrium geometry. Indeed, Δ_e^{gs} is missed[1,2] due to experimental difficulties and limitations of signal detection in the long wavelength spectral range.

(b) Q_θ-mode configuration energy diagram illustrating the ground and excited states splittings responsible for the emission and excitation band structure. Note that Δ_e^{es} is slightly smaller than Δ_t^{gs} in spite of $\Delta_e^{gs} > \Delta_t^{gs}$ ($\Delta_e^{gs} = 3.1\ \Delta_t^{gs}$ from Fig. 4 of the manuscript).

Adapted from Figure 1 of reference[2] with permission of Elsevier Publishing, 1989.

2. Electron Paramagnetic Resonance of $(CH_3NH_3)_2CdCl_4$: Cu^{2+}: temperature dependence of the gyromagnetic principal values.

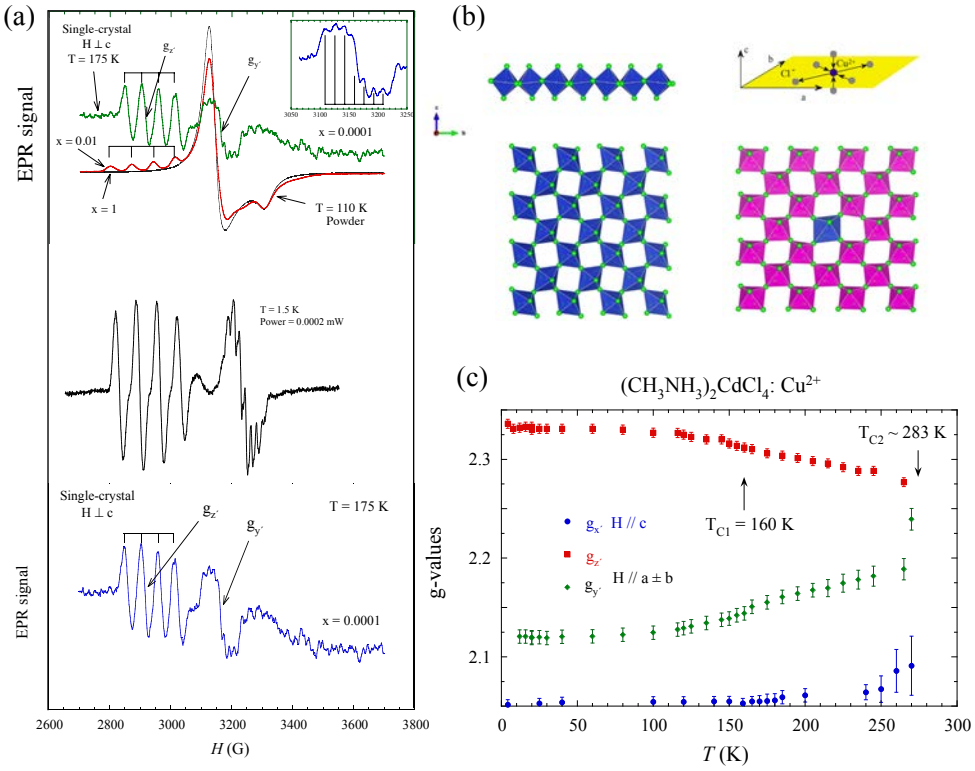

Figure S2

EPR spectra of Cu^{2+} introduced as a substitutional impurity in the layer perovskite $(CH_3NH_3)_2CdCl_4$.

(a) The plot shows the Cu^{2+} concentration dependence of single crystals of $(CH_3NH_3)_2(Cd_{1-x}Cu_x)Cl_4$ for *x* = 0.0001, 0.01, and 1 (pure copper crystal) at 175 K (single crystal) and 110 K (powder). Note that the spectra for the pure copper sample were obtained in single crystal and powder for comparison purposes. Besides the characteristic exchange averaged EPR spectra for x = 1, the characteristic signal of isolated Cu^{2+} become visible on decreasing the Cu^{2+} concentration. Only Cu^{2+} monomers are observed for x= 0.0001, while a mixture of monomers and aggregated phases are observed for intermediate concentrations. The lower the Cu^{2+} concentration the higher monomer to aggregate ratio. The monomer EPR spectrum (x = 0.0001) with the magnetic field applied perpendicular to the *a,b* plane of the layered perovskite is shown at 175 K (Tetragonal (*P4₂/n*cm) and 15 K (Monoclinic *P2₁/b*).[3-4] The local gyromagnetic values $g_{z'}$ and $g_{y'}$ are indicated. The in-plane elongated Cu-Cl bond is along z, while the two short Cu-Cl bonds are along y (nearly in *a,b* plane) and x (nearly perpendicular to plane, or parallel to *c*).

(b) Schematic representation of the Cu^{2+} local structure in pure $(CH_3NH_3)_2CuCl_4$ (left) and $(CH_3NH_3)_2CdCl_4$:Cu^{2+} (right). Note that the impurity system resembles the antiferrodistortive structure exhibited by the pure crystal but monomer displays a dynamical Jahn-Teller distortion among these two locally elongated coordination geometries.

(c) Variation of the principal gyromagnetic values of Cu^{2+} monomer with temperature. It must be noted that in the time scale of GHz radiation (10^{-9} s) the equilibrium geometry of Cu^{2+} corresponds to a rhombic local coordination geometry with the two nearly in-plane elongated Cu-Cl bonds with g_z = 2.33, and the two short Cu-Cl bonds associated with g_y = 2.12 (nearly in plane larger bond) and g_x = 2.055 (nearly perpendicular to the crystal layer). The g values change with temperature according to a dynamically-induced geometrical exchange between the two in-plane elongated geometries. The in-plane g_y values evolve up to collapse to an average value $g_{z,y}$ = 2.24, while g_x varies from 2.055 to 2.09 at high temperature, reflecting the actual nearly tetragonal symmetry at Cd^{2+} site. Interestingly, the variation of the principal g-values with the temperature, which are mainly governed by the energy barrier associated with the two in-plane elongated dynamical configurations, is affected by the structural phase transition sequence of the host crystal $(CH_3NH_3)_2CdCl_4$. This sequence favors the trend to a dynamically averaged configuration towards higher temperature phases. The energy barrier tends to decrease along the phase transition sequence: Monoclininc (*P2₁/b*) – 160 K– Tetragonal (*P6₂/n*cm) – 283 K – Orthorhombic (*Abma*).[3-6]

3. Electron Paramagnetic Resonance of $(C_3H_7NH_3)_2CdCl_4$:Cu^{2+}: temperature dependence of the gyromagnetic principal values.

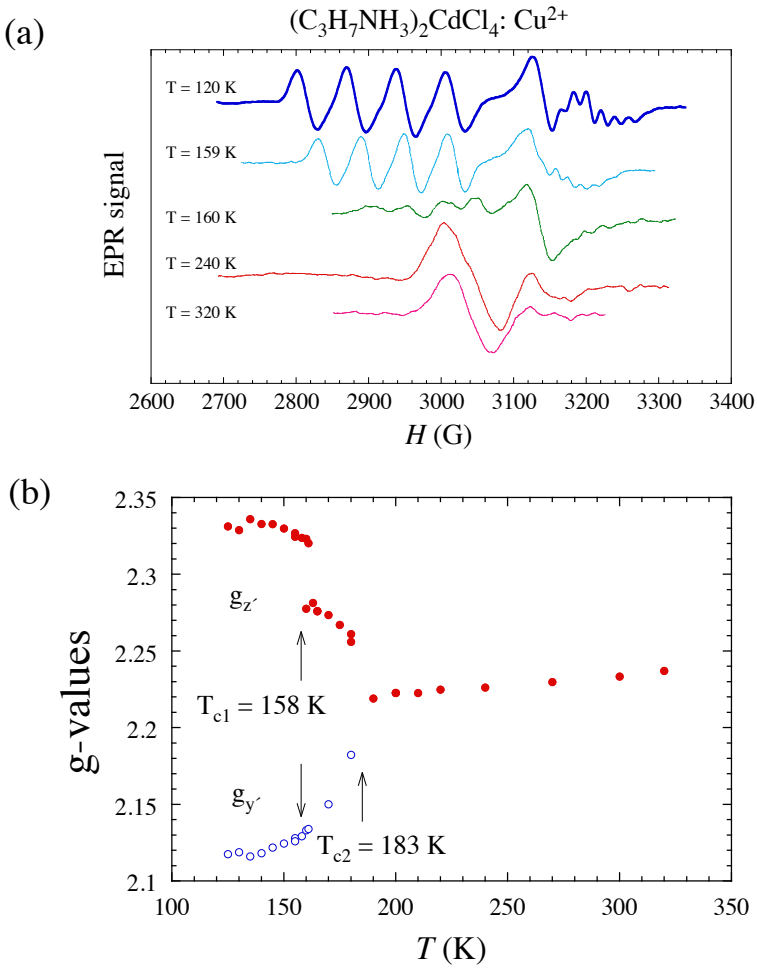

Figure S3

(a) EPR spectra and (b) gyromagnetic values of Cu^{2+} introduced as a substitutional impurity in the layer perovskite $(C_3H_7NH_3)_2CdCl_4$ as a function of temperature.

EPR spectra of diluted $(C_3H_7NH_3)_2CdCl_4$:Cu^{2+} taken with the magnetic field perpendicular to the *a,b* plane of the layered perovskite (Orthorhombic *Pbca* at 120 K)[7] at different temperatures between 120 K and 320 K. Note that the low temperature spectrum exhibits the hyperfine and superhyperfine structures characteristic of a Cu^{2+} monomer hexacoordinated by six Cl^- with two nearly in-plane elongated Cu-Cl bonds (g_z = 2.33) and two short Cu-Cl bonds, one nearly in-plane (g_y = 2.12) and the other one nearly perpendicular to plane (along *c*). Interestingly, the evolution of the EPR spectra with temperature renders a nice example of a 2D dynamical Jahn-Teller effect between the two equivalent in-plane elongated Cu^{2+} geometries which are stabilized when Cu^{2+} replaces Cd^{2+} at the compressed Cd^{2+} site (the four long Cd-Cl bonds lie in the *a,b* plane while the two sort Cd-Cl bonds correspond to terminal ligands aligned perpendicular to it –nearly along *c*–).[7-10]

Similar to the isomorphous $(C_3H_7NH_3)_2CdCl_4$, the evolution of the g values with temperature reflects the 2D dynamical Jahn-Teller effect tending to converge to an average g -value when the thermally activated exchange rate is shorter than the time scale of the microwave radiation (X-band). Nevertheless, the energy barrier associated with the dynamical exchange for Cu^{2+} in $(C_3H_7NH_3)_2CdCl_4$ is smaller than those attained in $(C_3H_7NH_3)_2CdCl_4$ where averaged spectra are observed above 283 K. In present $(C_3H_7NH_3)_2CdCl_4$:Cu^{2+}, we do also observe an abrupt reduction of g_z and a concomitant jump of g_y at the structural phase transition of the host: Orthorhombic (*Pbca*) – 158 K – Orthorhombic incommensurate with $\boldsymbol{q} \approx 0.42\boldsymbol{b^*}$ (*Abma*),[7,11,12] and a complete collapse at the structural phase transition to the Orthorhombic commensurate (*Abma*) phase at 183 K.[11,12] Given that transition temperatures in $(CH_3NH_3)_2CdCl_4$ are lower than corresponding transition temperatures in $(CH_3NH_3)_2CdCl_4$ we conclude that energy barriers for dynamical exchange are reduced in the propylammonium crystal with respect to methylammonium one.

4. Electron Paramagnetic Resonance of $(C_2H_5NH_3)_2CdCl_4$: Cu^{2+}: temperature dependence of the gyromagnetic principal values and ferromagnetic resonance

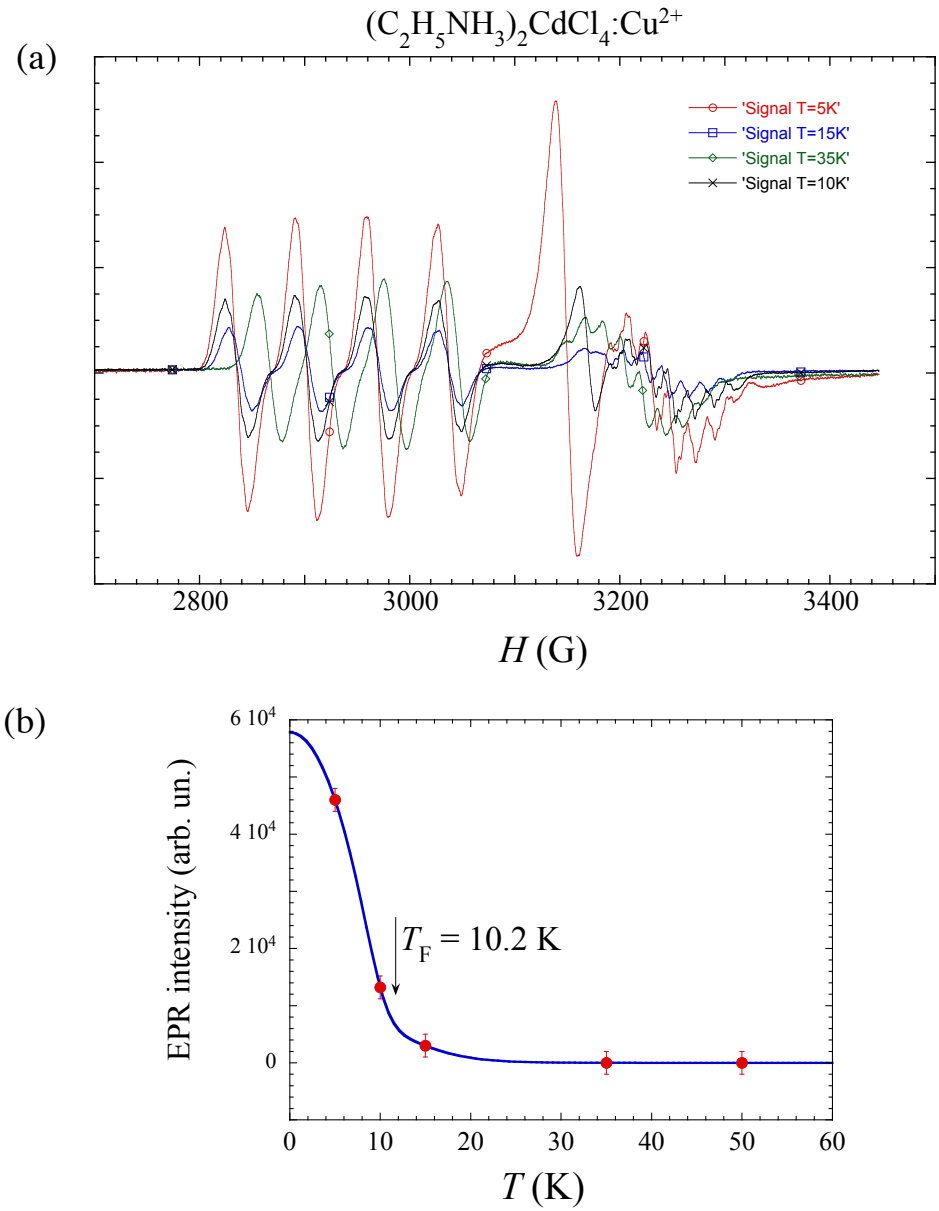

Figure S4

Structural characterization of Cu^{2+} introduced as a substitutional impurity in the layer perovskite $C_2H_5NH_3CdCl_4$ by means of EPR.

EPR spectra of diluted $(C_2H_5NH_3)_2CdCl_4:Cu^{2+}$ taken with the magnetic field perpendicular to the *a,b* plane of the layered perovskite (Monoclinic $B2_1/a$)[13] at different temperatures between 5 K and 35 K (a). This Monoclinic phase is stable up to 114 K.[13-16] Note that similar to $(CH_3NH_3)_2CdCl_4:Cu^{2+}$ and $(C_3H_7NH_3)_2CdCl_4:Cu^{2+}$, the low temperature spectrum of $(C_2H_5NH_3)_2CdCl_4:Cu^{2+}$exhibits the hyperfine and superhyperfine structures characteristic of a Cu^{2+} monomer hexacoordinated by six Cl^- with two nearly in-plane elongated Cu-Cl bonds (g_z = 2.33) and two short Cu-Cl bonds, one nearly in-plane (g_y = 2.12) and the other one nearly perpendicular to the crystal layer. Besides the 2D dynamical Jahn-Teller effect at higher temperatures, a relative intense single EPR peak is observed below 10 K (b). We associate this peak with a ferromagnetic resonance coming from marginal small $(C_2H_5NH_3)_2CuCl_4$ aggregates. This interpretation is based on the fact that this kind of aggregates are formed upon increasing the Cu^{2+} concentration, the exchange-narrowed gyromagnetic ratio (the ferromagnetic resonance magnetic field) increases (decreases) with decreasing temperature below the Curie temperature, which is T_F.= 10.2 K for bulk $(C_2H_5NH_3)_2CuCl_4$.[17,18] The line intensity falls down at the Curie temperature. The variation of $I(T)$ suggest that the actual Curie temperature might be a few degrees higher than bulk probably due to the small size of aggregates or the slightly lower exchange interactions provoked by the larger $(C_2H_5NH_3)_2CdCl_4$ lattice in comparison to $(C_2H_5NH_3)_2CuCl_4$.

5. Jahn-Teller and crystal anisotropy (stress) effects on the local structure of MX_6 (M: Cu^{2+}, Mn^{3+}; X: F^-, Cl^-) in ABX_3:M perovskite-type structures.

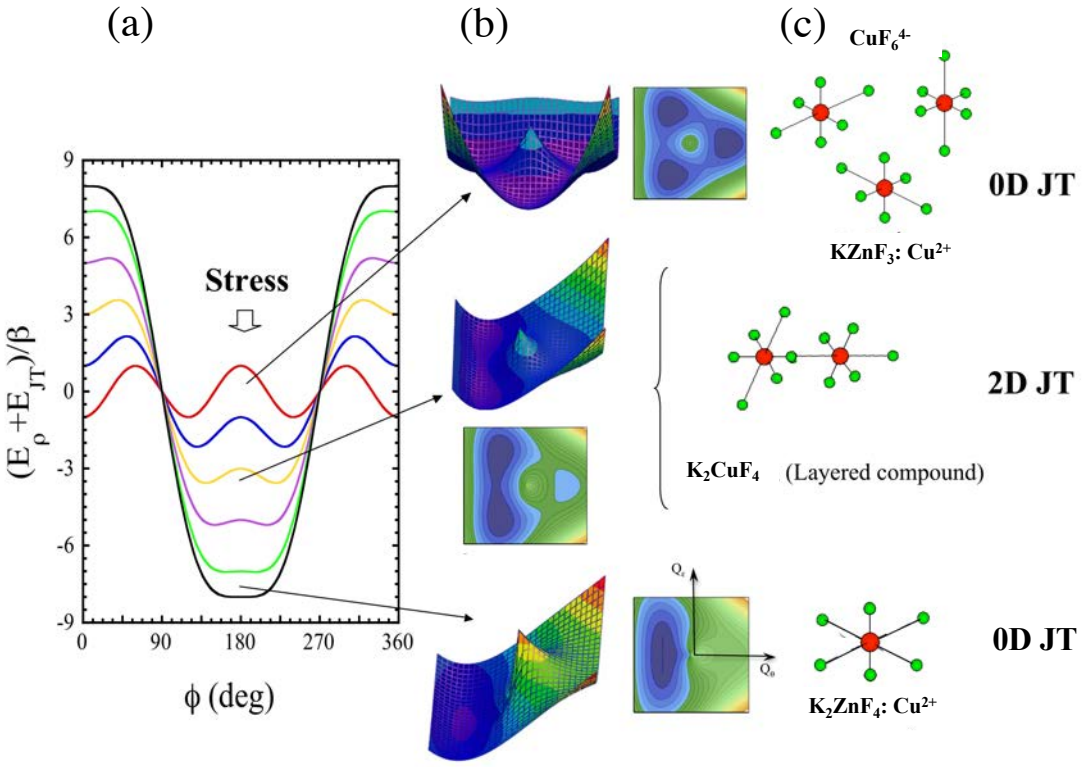

Figure S5
(a) Effect of crystal anisotropy represented through an effective axial stress in the ground-state energy in (Q_θ,Q_ε)-space given by the $E\otimes e$ Jahn-Teller theory.[10,18-20] (b) (Q_θ,Q_ε)-space ground-state energy surface. Note the evolution from elongated-to-compressed coordination geometry upon increasing the axial stress. The collapse into the compressed geometry takes place at $S_{crit} = 9\beta$. The parameter β (> 0 for elongated geometry minima) contains anharmonic and second-order JT interactions yielding warping of the Mexican-hat-type energy surface in (Q_θ,Q_ε)-space. 2β corresponds to the energy barrier for jumping among energy minima at $S = 0$. (c) Structures illustrate the CuF_6^{4-} equilibrium geometries predicted by the perturbed JT model.[18-20] The stress parameter is introduced in the Jahn-Teller model as $S = \pm A_e \rho_0$, with A_e and ρ_0 being the electron-lattice coupling constant associated with the $E\otimes e$ Jahn-Teller effect and the low-symmetry coordinate at the host site with plus or minus depending on whether the type of tetragonal distortion is compressed (compressive stress) or elongated (tensile stress), respectively.[20]

SI References

[1] Dubicki, L.; Riley, M. J.; Krausz, E. R. Electronic Structure of the Copper(II) Ion Doped in Cubic $KZnF_3$. *J. Chem. Phys.* **1994**, *101*, 1930.

[2] Dubicki, L.; Krausz, E. R.; Riley, M. J.; Yamada, I. Structured d-d Fluorescence from CuF_6^{4-} Doped in Cubic and Tetragonal Perovskites. *Chem. Phys. Lett.* **1989**, *157* (4), 315–320.

[3] Valiente, R.; Rodriguez, F. Polarized Electronic Spectra of the $(CH_3NH_3)_2Cd_{1-x}Mn_xCl_4$ (x = 0–1) Perovskite Layer Doped with Cu^{2+}: Study of the Cl^- to Cu^{2+} Charge Transfer Intensity Enhancement along the Series. *J. Phys. Chem. Sol.* **1996**, *57*, 571–587.

[4] Chapuis, G.; Arend, H.; Kind, R. X-Ray Study of the Structural First-order Phase Transition (Cmca-P4$_2$/ncm) in $(CH_3NH_3)_2CdCl_4$. *Phys. Stat. Sol.* **1975**, *31*, 449–454.

[5] Mokhlisse, R.; Couzi, M. .; Lassegues, J. C. Lattice Dynamics and Structural Phase Transitions in Perovskite-Type Layer Compounds. I. The Low-Frequency Inelastic Neutron Scattering and Raman Spectra of the Ordered Monoclinic Phase of $(CH_3NH_3)_2MnCl_4$ and $(CH_3NH_3)_2CdCl_4$. *J. Phys. C Solid State Phys.* **1983**, *16*, 1353–1366.

[6] Mokhlisse, R.; Couzi, M.; Loyance, P. L. Lattice Dynamics and Structural Phase Transitions in Perovskite-Type Layer Compounds. I. The analysis of the temperature-dependent Raman spectra of $(CH_3NH_3)_2CdCl_4$. *J. Phys. C Solid State Phys.* **1983**, *16*, 1367–1384.

[7] Ecolivet, C.; Kusto, W. Brillouin scattering in $(C_3H_7NH_3)_2CdCl_4$. *Ferroelectrics* **1990**, *125*, 285–290.

[8] Valiente, R.; Rodríguez, F.; Moreno, M.; Lezama, L. Vibronic Interactions: Jahn-Teller Effect in Crystals and Molecules; NATO Science Series, 2001; pp 221–228.

[9] Hitchman, M. A. The Influence of Vibronic Coupling on the Spectroscopic Properties and Stereochemistry of Simple 4- and 6- Coordinate Copper (II] Complexes. *Comments Inorg. Chem.* **1994**, *15* (3–4), 197–254.

[10] Rodríguez, F. Unveiling the Local Structure of Cu^{2+} Ions from D-Orbital Splitting. Application to $K_2ZnF_4:Cu^{2+}$ and $KZnF_3:Cu^{2+}$. *Inorg. Chem.* **2017**, *56* (4), 2029–2036.

[11] Chapuis, G. Study of the first-order phase transition of $(C_3H_7NH_3)_2CdCl_4$ at 183 K by X-ray diffraction of the two phases, *Acta Cryst. B* **1978**, 34,1506–1512.

[12] Doudin, B.; Chapuis, G. Study of the Modulated Phase of $(C_3H_7NH_3)_2CdCl_4$ by X-ray diffraction, *Acta Cryst. B* **1988**, 44,495-502.

[13] Hagemann, H.; Bill, H. Raman investigation on structural phase transitions in $(C_2H_5NH_3)_2CdCl_4$, *Chem Phys. Lett.* **1982**, 93, 582-585.

[14] Mohamed, C.B.; Karoui, K.; Saidi, S.; Guidara, K.; Rhaiem, A.B. Electrical properties, phase transitions and conduction mechanisms of the $[C_2H_5NH_3)_2CdCl_4$ compound. *Physica B* **2014**, *451*, 87–95.

[15] Yadav, R.; Swain, D.; Kundu, P.P.; Nair, H.S.; Narayana, C.; Elizabeth, S. Dielectric and Raman investigations of structural phase transitions in $(C_2H_5NH_3)_2CdCl_4$. *Phys. Chem. Chem. Phys.* **2015**, *17*, 12207–12214.

[16] Lefi, R.; Naser, F.B.; Guermazi, H. Structural, optical properties and characterization of $(C_2H_5NH_3)_2CdCl_4$, $(C_2H_5NH_3)_2CuCl_4$ and $(C_2H_5NH_3)_2Cd_{0.5}Cu_{0.5}Cl_4$ compounds. *J. Alloys Compd.* **2017**, *696*, 1244–1254.

[17] De Jongh, L. J.; Botterman, A. C.; De Boer, F. R.; Miedema, A. R. Transition Temperature of the Two-Dimensional Heisenberg Ferromagnet with S=1/2. J. Appl. Phys. **1960**, 40, 1363–1365.

[18] Aguado, F.; Rodríguez, F.; Valiente, R.; Señas, A.; Goncharenko, I. Three-dimensional magnetic ordering in the Rb_2CuCl_4 layer perovskite—structural correlations. *J. Phys.: Condens. Matter* **2004**, 16, 1927–1938.

[19] Rodríguez, F.; Aguado, F. Correlations between Structure and Optical Properties in Jahn–Teller Mn^{3+} Fluorides: A Study of $TlMnF_4$ and $NaMnF_4$ under Pressure. *J. Chem. Phys.* **2003**, *120*, 10867–10875.

[20] Aguado, F.; Rodríguez, F.; Valiente, R.; Itié, J. P.; Munsch, P. Pressure-Induced Jahn-Teller Suppression in $Rb_2CuCl_4(H_2O)_2$: Pseudo-Jahn-Teller Effect. *Phys. Rev. B* **2004**, *70*, 214104 (9 pages).